JOURNAL OF COMPUTATIONAL PHYSICS 10, 133–150 (1972)

Computation of Stable Equilibria in Minimum-**B** Mirror Devices*

DAVID V. ANDERSON†

JOHN KILLEEN

Lawrence Livermore Laboratory, University of California, Livermore, California 94550
and
Department of Applied Science, University of California, Davis, California 95616

Received November 2, 1971

We present a three-dimensional code that solves for plasma equilibria in open-field geometries, which allows analysis of most minimum-B mirror systems. Open confinement with $p = p(B)$ only requires the hydromagnetic equilibrium equation to reduce to one elliptic, scalar partial differential equation involving a tensor pressure. The finite difference form of the equation is solved by an implicit iterative algorithm similar to the ADI (alternating direction implicit) method. Cylindrical grid coordinates are employed, and the mesh spacing is variable to allow representation of far boundary conditions. We have time-optimized the program, so the memory requirements are large. It is found that, when the threshold for hydromagnetic instability is passed, the hydromagnetic equilibrium equation becomes hyperbolic, which leads to an ill-posed problem as predicted by Grad. Equilibria are found for an increasing sequence of pressures until the instability threshold is reached. The present code utilized planes of inversion symmetry common to many minimum-B devices, to allow a reduction in the domain to be studied; Ioffe bar devices, Baseball II, 2X-II, and the proposed mirror fusion experiment are representable. We present sample results for Baseball II and the Ioffe bar device, including cases near the high beta instability threshold.

1. INTRODUCTION

Computation of finite-beta plasma equilibria has up to now been restricted to configurations sharing the common feature of effective two-dimensional symmetry. We have developed a three-dimensional code that solves for plasma equilibria in open-field geometries.

The class of problems that can be solved by this three-dimensional code includes configurations in which the field lines are open and hence in which tensor pressure is required, to have equilibria. The hydromagnetic stability analysis, which is

* Work performed under the auspices of the U. S. Atomic Energy Commission.
† Present address: U.S. Naval Research Laboratory, Washington, DC 20390.

difficult for the scalar pressure systems in axially symmetric configurations, is comparatively simple here and can be performed by inspection of the equilibrium solution.

The model assumes complete charge neutrality, and we consider time-independent phenomena only. For this case Maxwell's equations reduce to the pair

$$\nabla \times \mathbf{B} = \mathbf{j} \tag{1}$$

$$\nabla \cdot \mathbf{B} = 0. \tag{2}$$

A tensor pressure model of the plasma is chosen for a class of equilibria in which $\mathsf{p} = \mathsf{p}(B)$ alone. Hydromagnetic equilibrium is given by the usual equation

$$\mathbf{j} \times \mathbf{B} = \nabla \cdot \mathsf{p}. \tag{3}$$

In presenting the results we will quote a value for β. We shall use the convention due to Post [1] and define a local β:

$$\beta = \frac{2p_\perp}{B_{\text{vac}}^2 + 2p_\perp} < 1. \tag{4}$$

The code has been set up such that it is easy to change the vacuum field of the mirror device so that we are able to study configurations such as Baseball II, 2X-II, a Ioffe bar machine, or almost any conceivable minimum-B device. The results we show are primarily of the Baseball II and Ioffe bar configurations. We look at several pressure models and compute the maximum pressure consistent with hydromagnetic stability.

2. Hydromagnetic Equilibrium Equation for Tensor Pressure

Systems with open field lines achieve plasma confinement by the mirror effect. Particles entering the velocity space loss cone are lost and there is thus no possibility of an isotropic distribution function. The pressure then is a tensor with two independent components $p_\perp$ and $p_\parallel$, where

$$\mathsf{p} = p_\perp \mathsf{I} + (p_\parallel - p_\perp)\,\mathbf{nn}$$

and

$$\mathbf{n} = \mathbf{B}/|B|; \qquad \mathsf{I} \text{ is the unit tensor.} \tag{5}$$

2.1. *Models for the Pressure Profile*

When considering what variables should be admitted to the arguments of p, we must restrict ourselves to models that can satisfy the equilibrium and that

correspond to a confined plasma. Profiles of the form $\mathsf{p} = \mathsf{p}(\psi)$, where ψ is a flux function, are excluded because it requires p to be constant on each flux tube, which is compatible with an infinite plasma only. Combinations of ψ with other variables may be admissible. The form of the pressure function depends ultimately on the assumed form of the particle distribution function. One possible choice is to choose profiles of the form $\mathsf{p} = \mathsf{p}(B)$. Taylor [2] has shown that the class of equilibria given by this choice allows one to considerably simplify the analysis. Northrop and Whiteman [3] have shown that the assumption of dependence on B only is equivalent to requiring that the guiding center distribution function be independent of the longitudinal invariant. Of many possible choices for this distribution function, one form given by Taylor [2] is

$$\begin{aligned} f(\mu, \epsilon) &= (\mu B_0 - \epsilon)^{m-3/2}\, g(\mu), \qquad \epsilon < \mu B_0 \\ f(\mu, \epsilon) &= 0, \qquad\qquad\qquad\quad \epsilon > \mu B_0\,, \end{aligned} \tag{6}$$

where μ and ϵ are the magnetic moment and the energy, respectively; these are constants of the motion for guiding center equilibria. The function g and the index $m > 2$ are arbitrary. Lower values of m can be shown to lead to instability in the zero β limit. B_0 is the value of B on the plasma boundary which is the value of B on the last closed contour of B. In the computations it is often convenient to take a somewhat smaller value for B_0. B_0 can be thought of as the level to which plasma can fill the well. In the same reference, Taylor also introduced the pressure functions

$$\left.\begin{aligned} p_\parallel &= CB(B_0 - B)^m \\ p_\perp &= CB^2 m(B_0 - B)^{m-1} \end{aligned}\right] \; B < B_0 \text{ and interior to the } B = B_0 \text{ surface}$$

$$p_\parallel = p_\perp = 0, \qquad \text{otherwise.} \tag{7}$$

These pressures can be obtained from any distribution function of the form given in Eq. (6). Other distribution functions can also integrate to this form.

2.2. *Equilibrium Equation for a Class of Equilibria*

The equilibrium equations can be reduced to [3, 4]

$$\mathbf{B} \times (\nabla \times (\nu \mathbf{B})) = 0 \tag{8}$$

or

$$\nabla \times \nu \mathbf{B} = k\mathbf{B}$$

for some scalar k, where we define

$$\nu = \frac{p_\parallel - p_\perp}{B^2} - 1. \tag{9}$$

From Eq. (8) we obtain the current

$$\mathbf{j} = (k/\nu)\mathbf{B} - (1/\nu)\,\nabla\nu \times \mathbf{B} \tag{10}$$

and

$$\nabla \cdot (\nabla \times \nu\mathbf{B}) = \nabla \cdot k\mathbf{B} = \mathbf{B} \cdot \nabla k = 0.$$

Since each field line leaves the plasma boundary, the current along that line must vanish at the boundary. That is $k = 0$ at the boundary. The condition $\mathbf{B} \cdot \nabla k = 0$ ensures that $k \equiv 0$ inside the plasma, also. From Eq. (8) we obtain the equation

$$\nabla \times \nu\mathbf{B} = 0. \tag{11}$$

We define a potential by

$$\nu\mathbf{B} = \nabla\phi \tag{12}$$

so then $(\nabla \cdot \nu\mathbf{B}) = \nabla^2\phi = \mathbf{B} \cdot \nabla\nu$. The scalar equation

$$\nabla^2\phi = \frac{1}{\nu}\,\nabla\phi \cdot \nabla\nu \tag{13}$$

then represents the equilibrium.

The decomposition $\phi = \phi_c + \phi_p$ is made in which ϕ_c denotes the contribution of the vacuum field which is given and ϕ_p is the unknown potential function giving the plasma fields. For a vacuum, then,

$$\nabla^2\phi_c = 0, \qquad \mathbf{B}_c = -\nabla\phi_c\,, \qquad \text{and} \qquad \nu_c = -1. \tag{14}$$

Using Eq. (14) in Eq. (13) allows one to pose the problem in terms of the plasma contribution ϕ_p alone. So the equation to be solved numerically is

$$\nabla^2\phi_p = (1/\nu)[\nabla\nu \cdot (\nabla\phi_p - \mathbf{B}_c)], \tag{15}$$

which is of elliptic form.

2.3. *Boundary Conditions on the Plasma Fields*

The basic boundary condition is $\phi_p = 0$ on a surface far from the plasma. That is, at some finite but large distance from the plasma we neglect the fields produced by the plasma. Errors of a few percent, in our experience, result from these approximate boundary conditions.

We have thus far made no assumptions about the symmetry of the configuration, so Eq. (15) is applicable to any open geometry of interest. For the confinement

schemes considered, we shall use cylindrical coordinates r, z, θ. In practice, one makes use of other symmetries such as inversion symmetry to reduce the full domain.

2.4. *Hastie–Taylor Criteria for Hydromagnetic Stability*

For collisional tensor pressure plasmas, Bernstein [5] gives the double adiabatic energy principle; if we are interested in collisionless plasmas, then the energy principle of Kruskal and Oberman [6] is the appropriate one to use. It has been shown that this latter criterion for stability is always more pessimistic, that is [7],

$$\delta W_{KO} < \delta W_{DA}\,, \tag{16}$$

where DA refers to the double adiabatic model. Taylor had worked out sufficient conditions for stability in terms of the double adiabatic energy principle, but it clearly does not apply in the collisionless case [2]. Taylor and Hastie [8] later obtained necessary and sufficient conditions for the stability of a collisionless guiding center plasma, which are then also sufficient conditions for the stability of a collisional model. They obtained their result for the class of equilibria discussed earlier, where $p_\perp = p_\perp(B)$ and $p_\parallel = p_\parallel(B)$.

The collisionless guiding center model, with μ and ϵ constants of the particle motion, is used with the energy principle of Kruskal and Oberman. After performing the algebra and considering distribution functions of the form

$$(\partial f/\partial \epsilon) < 0, \tag{17}$$

one arrives at the following inequalities:

$$B - p_\parallel{}' > 0 \qquad \text{and} \qquad B + p_\perp{}' > 0. \tag{18}$$

These two conditions are referred to as the necessary and sufficient conditions of Taylor and Hastie [8] for hydromagnetic stability. The first of these conditions is equivalent to

$$\nu < 0. \tag{19}$$

when $p_\perp(B)$ and $p_\parallel(B)$ are given by Eq. (7).

Physically one can show that this is the requirement that the firehose mode be stable. The other requirement, $B + p_\perp{}' > 0$, is the condition in which the mirror instability is suppressed.

Grad [9] has shown that the character of the equilibrium equation changes from elliptic to hyperbolic wherever the Hastie–Taylor thresholds are exceeded.

3. Mirror Equilibrium Computational Methods

We now proceed to solve Eqs. (15) and (12) on a three-dimensional finite-difference grid.

The cylindrical form of Eq. (15) is

$$\frac{1}{r}\frac{\partial}{\partial r}\left(r\frac{\partial\phi}{\partial r}\right)+\frac{1}{r^2}\frac{\partial^2\phi}{\partial\theta^2}+\frac{\partial^2\phi}{\partial z^2}$$
$$=\frac{1}{\nu}\left[\frac{\partial\nu}{\partial r}\left(\frac{\partial\phi}{\partial r}-B_{r_c}\right)+\frac{1}{r^2}\frac{\partial\nu}{\partial\theta}\left(\frac{\partial\phi}{\partial\theta}-B_{\theta_c}\right)+\frac{\partial\nu}{\partial z}\left(\frac{\partial\phi}{\partial z}-B_{z_c}\right)\right], \quad (20)$$

where we have suppressed the subscript p, i.e., $\phi_p \rightarrow \phi$. Most proposed and existing mirror confinement devices possess planes of inversion symmetry. For the Ioffe bar devices [2] there are L of these planes located at

$$\theta = (l-1)(\pi/L) \qquad l = 1,\ldots, L, \quad (21)$$

where L gives the number of Ioffe bar pairs. For the devices Baseball II [10] and 2X-II [11], two mutually perpendicular inversion planes exist and hence have the same symmetry as an $L = 2$ Ioffe bar device, which is shown in Fig. 1. These symmetries allow one to study a reduced domain. In the r and z coordinates, the domain is not reduced; in θ, however, the full domain $(0, 2\pi)$ is reduced to $(0, \pi/L)$.

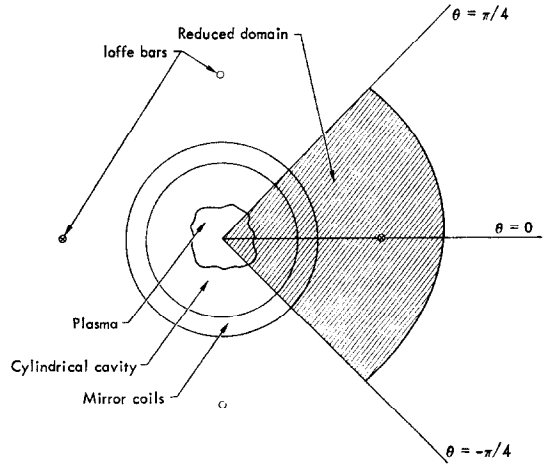

FIG. 1. End view of an $L = 2$ Ioffe bar device. Note that the domain may include the external coils. Inversion symmetry through the $\theta = \pi/4$ and the $\theta = -\pi/4$ planes allows reduction of the domain as shown. The same symmetries apply to Baseball II and the 2X-II experiments.

For Baseball II, then, the domain is $(0, \pi/2)$, which allows a fourhold reduction in the number of grid points required for the computation. An assumption implicit in what we have said here is the reasonable requirement that the plasma fields have the same symmetries as the vacuum fields.

To summarize, the domain for Baseball II is given by

$$\begin{aligned} 0 \leqslant r &\leqslant r_{\max} \\ -z_{\max} \leqslant z &\leqslant z_{\max} \\ 0 \leqslant \theta &\leqslant \pi/2. \end{aligned} \tag{22}$$

Then, coupling these symmetry conditions with the far-field boundary condition that the plasma fields be negligible at the outer boundaries, we arrive at the following boundary conditions:

$$\begin{aligned} \phi(r = r_{\max}) = 0 &= (\partial\phi/\partial r)(r = 0), \\ (\partial\phi/\partial\theta)(\theta = \pi/2) = 0 &= (\partial\phi/\partial\theta)(\theta = 0), \end{aligned} \tag{23}$$

and

$$\phi(z = z_{\max}) = 0 = \phi(z = -z_{\max}).$$

Equation (20), together with these boundary conditions, forms a well-posed computational problem; Eq. (12) represents an algebraic equation that allows us to evaluate ν as a function of ϕ. It also allows us to compute B.

When Eq. (20) is solved in two dimensions, the alternating direction implicit (ADI) method is used to obtain the solution. For three dimensions, the ADI scheme can produce numerical instabilities, and a generalization of it that is better behaved is used [12]. Instead, we use an algorithm developed by Douglas and Gunn [13] to solve Eq. (20).

Before the DG algorithm can be used, we convert Eq. (20) to a parabolic equation in which the time variable plays the role of iteration parameter. So, instead of solving Eq. (20), we solve the equation

$$\nabla^2\phi - (1/\nu)\,\nabla\nu \cdot (\nabla\phi - \mathbf{B}_c) = \partial\phi/\partial t, \tag{24}$$

and look for the steady state solutions which then satisfy Eq. (20) also.

For any orthogonal coordinate system the finite difference form of the equilibrium equations can be reduced to one scalar equation of the form

$$A\phi_{i-1} + B\phi_{i+1} + C\phi_{j-1} + D\phi_{j+1} + E\phi_{k-1} + F\phi_{k+1} + G\phi = g. \tag{25}$$

Here we have suppressed all the nonvaried subscripts, i.e., $A = A_{ijk}$, $\phi_{i-1} = \phi_{i-1,j,k}$, etc. The i, j, and k indices give the spatial location in terms of

the orthogonal coordinates x_1, x_2, and x_3, so $\phi_{ijk} = \phi[(x_1)_i, (x_2)_j, (x_3)_k]$. The coefficient G can be decomposed into the form $G = G_1 + G_2 + G_3$, where each successive term involves the i, j, k operators, respectively. We then define the generalized difference operators Δ_{x_1}, Δ_{x_2}, and Δ_{x_3} by

$$\Delta_{x_1}\phi = A\phi_{i-1} + B\phi_{i+1} + G_1\phi,$$

$$\Delta_{x_2}\phi = C\phi_{j-1} + D\phi_{j+1} + G_2\phi,$$

and

$$\Delta_{x_3}\phi = E\phi_{k-1} + F\phi_{k+1} + G_3\phi. \tag{26}$$

The difference equation corresponding to Eq. (20) is

$$(\Delta_{x_1} + \Delta_{x_2} + \Delta_{x_3})\,\phi = g. \tag{27}$$

Taking the finite difference form of Eq. (24), we get the difference equations

$$(\Delta_{x_1} + \Delta_{x_2} + \Delta_{x_3})\,\phi = g + \rho(\phi^{n+1} - \phi^n), \tag{28}$$

where $\rho = 1/\Delta t$, and is an iteration parameter. We must have $\rho > 0$. The superscript n or $n + 1$ is intentionally deleted from the LHS, and it is the DG algorithm that specifies the exact mixture of ϕ^{n+1} and ϕ^n to be used. The DG method is a three-step process. The first equation treats the Δ_{x_1} operator implicitly, and the other two equations treat Δ_{x_2} and Δ_{x_3} implicitly. The equations are

$$\tfrac{1}{2}\Delta_{x_1}(\phi^{n+1} + \phi^n) + \Delta_{x_2}\phi^n + \Delta_{x_3}\phi^n = g + \rho(\phi^{n+1} - \phi^n), \tag{29a}$$

$$\tfrac{1}{2}\Delta_{x_1}(\phi^{n+1} + \phi^n) + \tfrac{1}{2}\Delta_{x_2}(\phi^{n+2} + \phi^n) + \Delta_{x_3}\phi^n = g + \rho(\phi^{n+2} - \phi^n), \tag{29b}$$

and

$$\tfrac{1}{2}\Delta_{x_1}(\phi^{n+1} + \phi^n) + \tfrac{1}{2}\Delta_{x_2}(\phi^{n+2} + \phi^n) + \tfrac{1}{2}\Delta_{x_3}(\phi^{n+3} + \phi^n) = g + \rho(\phi^{n+3} - \phi^n). \tag{29c}$$

A more useful set is obtained by subtracting Eq. (29b) from Eq. (29a), and Eq. (29c) from Eq. (29b), so the set is

$$\tfrac{1}{2}\Delta_{x_1}(\phi^{n+1} + \phi^n) + \Delta_{x_2}\phi^n + \Delta_{x_3}\phi^n = g + \rho(\phi^{n+1} - \phi^n), \tag{30a}$$

$$\tfrac{1}{2}\Delta_{x_2}(\phi^{n+2} - \phi^n) = \rho(\phi^{n+2} - \phi^{n+1}), \tag{30b}$$

and

$$\tfrac{1}{2}\Delta_{x_3}(\phi^{n+3} - \phi^n) = \rho(\phi^{n+3} - \phi^{n+2}). \tag{30c}$$

Given ϕ^n, we solve Eq. (30a) for ϕ^{n+1} and use it sequentially to obtain ϕ^{n+2} and ϕ^{n+3} from Eqs. (30b) and (30c). We then set $\phi^{n+3} \to \phi^n$ and repeat until the iterative process converges. We check convergence by computing the residual error $| \phi^{n+3} - \phi^n |$.

Each of the equations is now a one-dimensional two-point boundary value problem in the x_1, x_2, and x_3 coordinate, respectively, and each is solved by the double-sweep algorithm. For example, we give the algorithm for Eq. (30a). Since ϕ^{n+1} is the unknown in the equation, we write it as

$$\Delta_{x_1}\phi^{n+1} - 2\rho\phi^{n+1} = 2g - \Delta_{x_1}\phi^n - 2(\Delta_{x_2} + \Delta_{x_3})\,\phi^n - 2\rho\phi^n = S\phi^n, \quad (31)$$

where $S\phi^n$ is shorthand for the right side, which is a known function. We now expand the Δ_{x_1} to obtain

$$A\phi_{i-1}^{n+1} + B\phi_{i+1}^{n+1} + G_1\phi_i^{n+1} - 2\rho\phi_i^{n+1} = S\phi^n. \quad (32)$$

Let

$$\phi_{i-1}^{n+1} = e_{i-1}\phi_i^{n+1} + f_{i-1} \quad (33)$$

and substitute this into Eq. (32). We obtain

$$\phi_i^{n+1} = \frac{-B}{(Ae_{i-1} + G_1 - 2\rho)}\,\phi_{i+1}^{n+1} + \frac{S\phi^n - Af_{i-1}}{(Ae_{i-1} + G_1 - 2\rho)}, \quad (34)$$

which is of the same form as Eq. (33), so we get

$$e_i = -B/(Ae_{i-1} + G_1 - 2\rho) \quad (35)$$

$$f_i = (S\phi^n - Af_{i-1})/(Ae_{i-1} + G_1 - 2\rho). \quad (36)$$

Equations (33), (35), and (36) give us the machinery to solve Eq. (31). The boundary condition at $i = 1$ is used to give e_1 and f_1. By sweeping to the right, using Eqs. (35) and (36), we generate the entire sequence of e's and f's. The upper boundary condition is used to determine $\phi_{I_{\max}}$. Then Eq. (33) is used in a sweep to the left to obtain the solution ϕ^{n+1} at each grid point. This equation is solved for each i line specified by a j, k pair of indices, except for those j, k pairs lying on the boundary surface. Equations (30b) and (30c) are solved in a similar manner. After each full iteration cycle (generating a ϕ^{n+3} from a ϕ^n), we must also change the coefficients A, B, C, D, E, and F, which are, in general, functions of ϕ. The function g must also be recomputed. These dependences on ϕ make the equations nonlinear.

If the equations were linear, then the DG algorithm is unconditionally stable in the numerical sense. Introduction of the nonlinearities may lead to cases in which stable convergence requires the convergence constant ρ to exceed some

critical value. In practice, where the nonlinearities are not too pathological, we usually obtain stable convergence to a solution.

For reference we give the values of the various difference coefficients. The indices i, j, and k refer to the coordinates, r, θ, and z, respectively. The differencing was done such that the difference equations are still valid on a nonuniform mesh. A restriction on the mesh is that the grid cells remain rectangular in the r, θ, z space. From Eq. (20) we get the following coefficients for Eq. (25):

$$A_{ijk} = \frac{(r_{i-1} + r_i)}{(r_{i+1} - r_{i-1})(r_i - r_{i-1})\, r_i} + \left(\frac{1}{\nu}\frac{\partial \nu}{\partial r}\right)_{ijk} \frac{1}{(r_{i+1} - r_{i-1})},$$

$$B_{ijk} = \frac{(r_i + r_{i+1})}{(r_{i+1} - r_{i-1})(r_{i+1} - r_i)\, r_i} - \left(\frac{1}{\nu}\frac{\partial \nu}{\partial r}\right)_{ijk} \frac{1}{(r_{i+1} - r_{i-1})},$$

$$C_{ijk} = \frac{2}{r_i^2} \frac{1}{(\theta_{j+1} - \theta_{j-1})(\theta_j - \theta_{j-1})} + \left(\frac{1}{\nu r^2}\frac{\partial \nu}{\partial \theta}\right)_{ijk} \frac{1}{(\theta_{j+1} - \theta_{j-1})},$$

$$D_{ijk} = \frac{2}{r_i^2} \frac{1}{(\theta_{j+1} - \theta_{j-1})(\theta_{j+1} - \theta_j)} - \left(\frac{1}{\nu r^2}\frac{\partial \nu}{\partial \theta}\right)_{ijk} \frac{1}{(\theta_{j+1} - \theta_{j-1})},$$

$$E_{ijk} = \frac{2}{(z_{k+1} - z_{k-1})(z_k - z_{k-1})} + \left(\frac{1}{\nu}\frac{\partial \nu}{\partial z}\right)_{ijk} \frac{1}{(z_{k+1} - z_{k-1})},$$

$$F_{ijk} = \frac{2}{(z_{k+1} - z_{k-1})(z_{k+1} - z_k)} - \left(\frac{1}{\nu}\frac{\partial \nu}{\partial z}\right)_{ijk} \frac{1}{(z_{k+1} - z_{k-1})},$$

$$G_{1_{ijk}} = \frac{-(r_i + r_{i+1})}{r_i(r_{i+1} - r_{i-1})(r_{i+1} - r_i)} - \frac{(r_{i-1} + r_i)}{r_i(r_{i+1} - r_{i-1})(r_i - r_{i-1})},$$

$$G_{2_{ijk}} = \frac{-2}{r_i^2}\left[\frac{1}{(\theta_{j+1} - \theta_{j-1})(\theta_{j+1} - \theta_j)} + \frac{1}{(\theta_{j+1} - \theta_{j-1})(\theta_j - \theta_{j-1})}\right],$$

$$G_{3_{ijk}} = -2\left[\frac{1}{(z_{k+1} - z_{k-1})(z_{k+1} - z_k)} + \frac{1}{(z_{k+1} - z_{k-1})(z_k - z_{k-1})}\right],$$

and

$$g_{ijk} = -\left[\frac{1}{\nu}\left(\frac{\partial \nu}{\partial r} B_{rc} + \frac{1}{r}\frac{\partial \nu}{\partial \theta} B_{\theta c} + \frac{\partial \nu}{\partial z} B_{zc}\right)\right]_{ijk}. \tag{37}$$

4. Computed Equilibria for Mirror Systems

4.1. *Ioffe Bar Equilibria*

The Ioffe bar model allows us to study a variety of magnetic wells; both the longitudinal mirror ratio and the radial profile of B may be varied independently. Understanding the effect of these parameters on the high beta equilibria may be useful in choosing designs for actual coil geometries. For example, the fields of Baseball II are more realistic but have the mirror ratio fixed at 2, and the radial

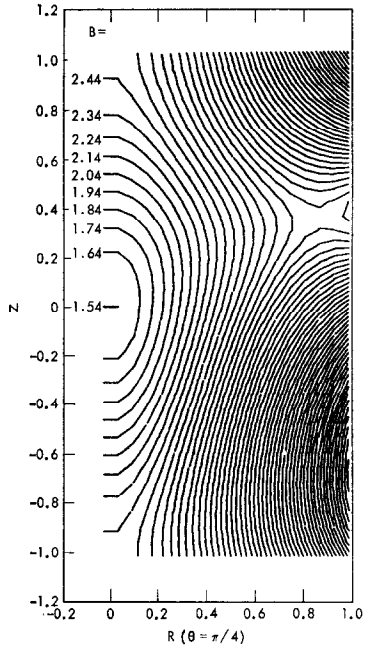

FIG. 2. Mod-B contours for the Ioffe bar vacuum field in the $\theta = \pi/4$ plane. At $\theta = -\pi/4$, the results are an inversion of these through $z = 0$. At $\theta = 0$, the results are symmetric about $z = 0$.

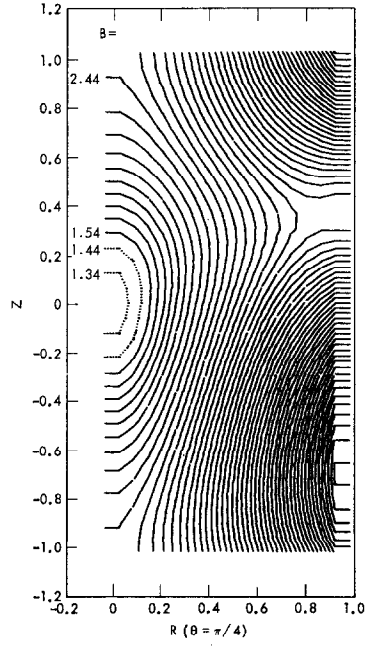

FIG. 3. Ioffe device equilibrium result for $m = 3$, $C = 0.1$, and $B_0 = 2.2$. The innermost solid contour is the minimum-B value of the vacuum field. The dotted contours show the deeper parts of the magnetic well carved out by the plasma. $\beta = 0.25$ at the center.

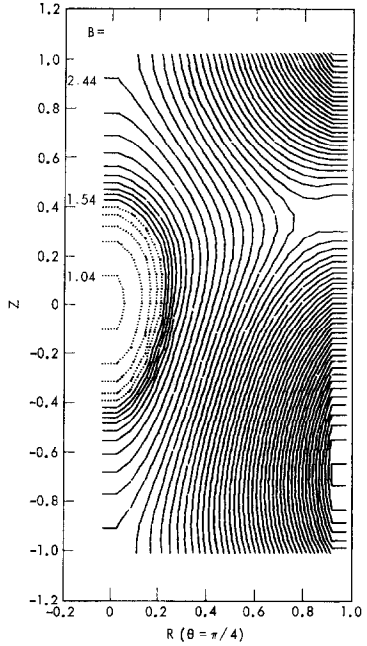

FIG. 4. Higher beta result for Ioffe device equilibrium for $m = 3$, $C = 0.2$, and $B_0 = 2.2$. Note the wiggles in the B contours in the region of large field gradients. Here $\beta = 0.42$ at the center and $\beta_c = 0.43$ gives the critical value corresponding to onset of the mirror instability.

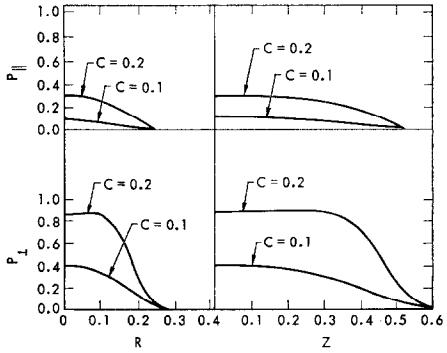

FIG. 5. Longitudinal and radial pressure profiles for the Ioffe device equilibria previously shown in Figs. 3 and 4. We note that $p_\perp$ has a very flat profile in the center region and has its maximum near the surface of the plasma.

profile is also fixed. So in spite of the somewhat ideal representation of the Ioffe bar fields, they do allow us some freedom in experimenting with the shape of the magnetic wells.

We present some sample graphical output of results in Figs. 2 through 5. The first figure shows the B contours for the vacuum field. Then the distorted equilibrium fields corresponding to a moderate and high beta are given. When the parameter C cas increased to 0.25, the solution diverged wildly. From the Hastie–Taylor criteria, Eq. (18), we can show that the mirror instability threshold is given by the critical value $C_c = 0.28$. The critical beta corresponding to this is $\beta_c = 0.43$. We also see that the gradients of B and $p_\perp$ are large in the region of the plasma surface; we can check that it is in this region that the mirror instability first occurs. We can also observe small ripples in Fig. 4; the wavelength of these ripples seems to be about 2 to 4 grid spacings long.

4.2. *Baseball II Experiment*

A tape of the Baseball II vacuum field has been prepared from the solution of the Biot–Savart law for the coil configuration. The field is fixed with respect to

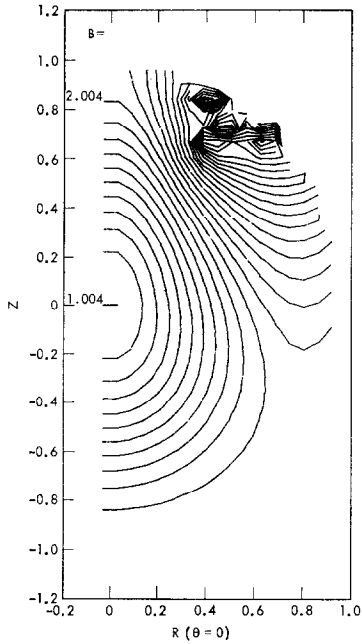

FIG. 6. Baseball II vacuum field B contours in the $\theta = 0$ plane. The unusual pattern in the upper right corner is due to the presence of the Baseball coils located there. The picture is inverted for the $\theta = \pi/2$ plane and it is symmetric about $z = 0$ for the $\theta = \pi/4$ plane. Here the mirror ratio is 2 and minimum-B = 1.0.

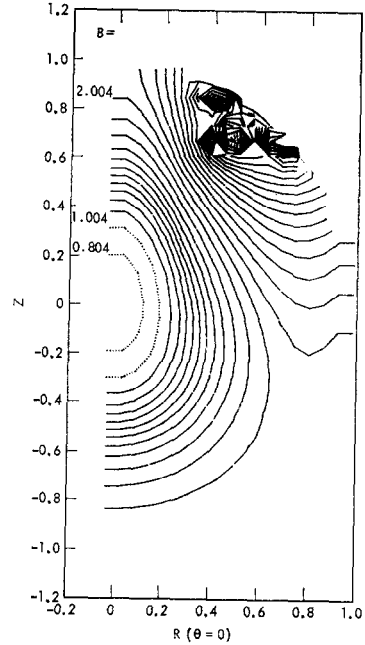

FIG. 7. Baseball II equilibrium field for $C = 0.20$, $m = 3$, and $B_0 = 1.8$. $\beta = 0.41$ at the center.

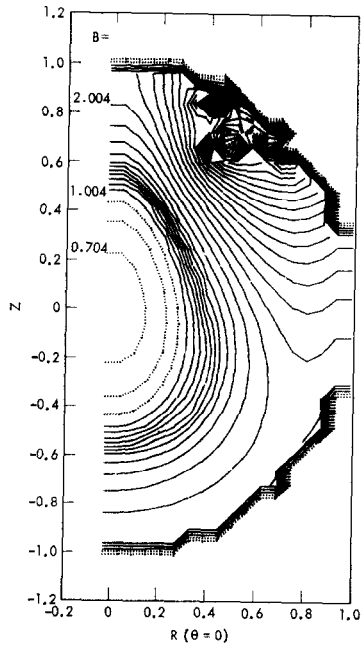

FIG. 8. Baseball II equilibrium field for $C = 0.33$, $m = 3$, and $B_0 = 1.8$. $\beta = 0.54$ at the center. The ripples are apparent now as we approach the mirror instability threshold.

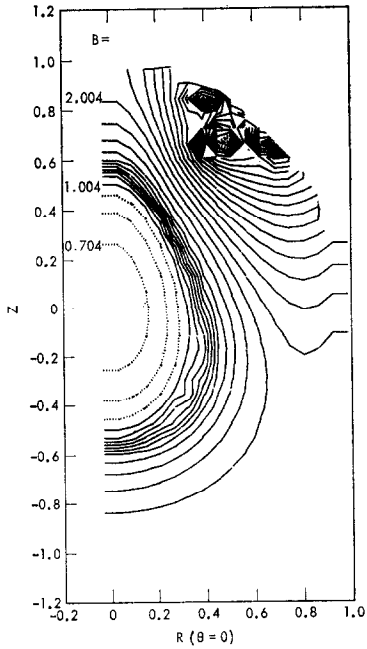

FIG. 9. Baseball II equilibrium field near the mirror instability threshold with $C = 0.36$, $m = 3$, and $B_0 = 1.8$. $= 0.55$ at the center. At the threshold the criteria of Hastie and Taylor give $C_c = 0.41$ and $\beta_c = 0.61$. The wiggles are very prominent here.

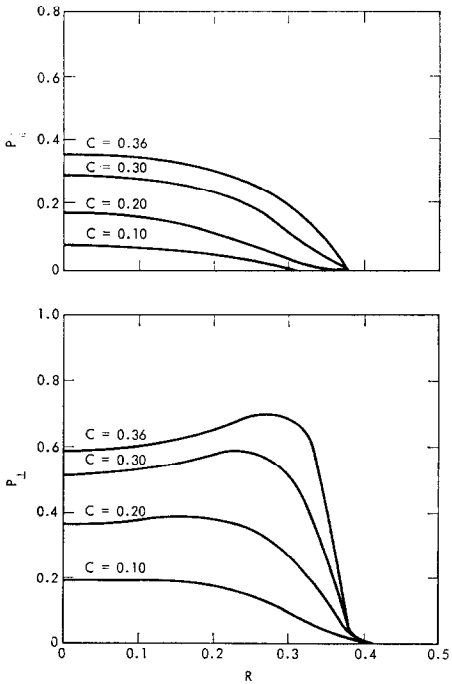

FIG. 10. Radial pressure profiles for Baseball II equilibria. Pressure values corresponding to the results shown in Figs. 7 and 9 are plotted. The $p_\perp$ profile now has a pronounced maximum near the plasma surface. β still takes its maximum value at the center however.

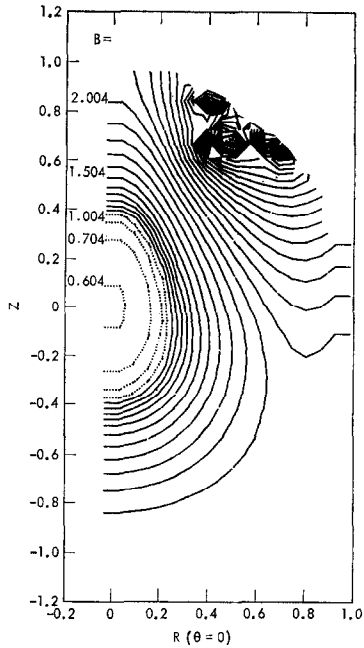

FIG. 11. Baseball II equilibrium field for $C = 0.2$, $m = 4$, and $B_0 = 1.8$. Compare this figure with Fig. 7 to see the m dependence. This equilibrium is near the mirror instability threshold. $\beta_e = 0.52$ and $\beta = 0.50$ at the center. $C_c = 0.25$. Again the ripples appear.

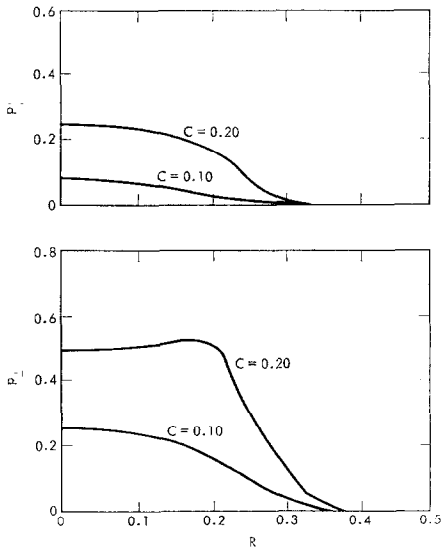

FIG. 12. Radial pressure profiles for Fig. 11.

mirror ratio and radial profile; it can be varied only by a scaling factor, which is of no interest here because the computation is in dimensionless variables. For convenience we have picked the dimensionless variables such that the minimum-B value is just 1. Since the mirror ratio is 2, the value of B on the last closed surface of constant B is 2. These values correspond to 20 kg and 40 kg, respectively, in the actual experiment.

Figures 6–9 give the equilibrium fields for a sequence of runs in which the pressure was increased until a value of the parameter C corresponded to a blowing-up solution. For this series of runs, all with the same values for m and B_0, $C = 0.40$ caused the solution to diverge. The theory predicts $\beta_c = 0.61$ and $C_c = 0.41$. Figure 10 gives the pressures.

Another set of runs was made for a different m value. Here $m = 4$, whereas it was 3 for the first set of runs. The results are shown in Figs. 11 and 12. The value $C = 0.25$ was sufficient to destroy the solution. The Hastie–Taylor criteria for the mirror instability give $C_c = 0.27$ and $\beta_c = 0.52$. The steep gradients and ripples are again prominent for the high beta limit.

5. Discussion

All of the results for high beta show $p_\perp$ having its maximum near the plasma surface rather than at the location of the minimum-B. One would not guess this result offhand, but it is clear from the form of Eq. (7) that the maximum occurs either at the minimum of B or at $B = 2B_0/(1 + m)$, according to which B is larger. The first of these is usually associated with low beta, whereas the second one obtains for the high beta equilibria.

It has been suggested by Grad [9] that unstable equilibria may not exist for open-confinement configurations. The apparent inability of our code to find unstable quilibria corresponds to this notion. The ripples are thought to be related to the loss of equilibrium at the mirror instability threshold.

The argument showing that unstable equilibria do not exist can be given if one examines the form of Eq. (20). We would guess from a first glance that this equation is of the elliptic form. The function ν depends on $\nabla\phi$, so there will be some second-order terms on the right side of Eq. (20) also. For sufficiently high beta, these terms become important and cause the equation to become hyperbolic in the region of the mirror instability. Keeping the same boundary conditions (essentially Dirichlet) leads to an ill-posed problem possessing no solution.

Other experimental configurations are easily studied simply by making a tape of the vacuum field. It is clear from the form of Eq. (20) that the vacuum field is only needed in the region of the plasma. The full domain is larger than the domain of the vacuum field, and it is on this that we solve the equilibrium equation. In

Fig. 13 we give a sketch of the relationships of the various domains and regions. Singularities in the expressions for the vacuum field do not cause a problem because the vacuum field is not computed in the coil region.

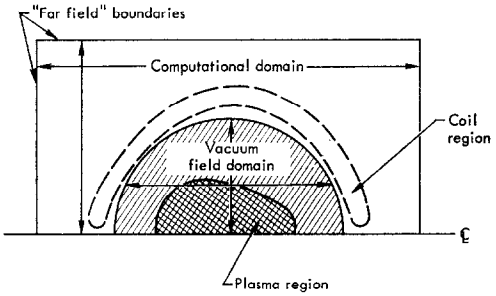

FIG. 13. This sketch shows the relationship of the computational domain to the domain of the vacuum field and to the plasma region. For the problems solved here the computational domain was not much larger than the vacuum field domain. Coils may be inside the computational domain so long as the plasma equilibrium surface does not touch them.

REFERENCES

1. R. F. POST, *Progr. Nucl. Energy Ser. II* **1** (1959), 154.
2. J. B. TAYLOR, *Phys. Fluids* **6** (1963), 1529.
3. T. G. NORTHROP AND K. J. WHITEMAN, *Phys. Rev. Lett.* **12** (1964), 639.
4. J. KILLEEN AND K. J. WHITEMAN, *Phys. Fluids* **9** (1966), 1846.
5. I. B. BERNSTEIN, E. A. FRIEMAN, R. M. KULSRUD, AND M. D. KRUSKAL, *Proc. Roy. Soc. London A* **244** (1958), 17.
6. M. D. KRUSKAL AND C. R. OBERMAN, *Phys. Fluids* **1** (1958), 275.
7. R. KULSRUD, Advanced Plasma Theory, in "Proc. Int. Sch. Phys. 'Enrico Fermi,' Course XXV," pp. 64–96, Academic Press, New York, 1964.
8. J. B. TAYLOR AND R. J. HASTIE, *Phys. Fluids* **8** (1965), 323.
9. H. GRAD, The Guiding Center Plasma, *Proc. AMS Symp. Appl. Math.* **18** (1967), 162.
10. K. H. BERKNER, W. S. COOPER, C. C. DAMM, K. W. EHLERS, A. H. FUTCH, G. W. HAMILTON, J. E. OSHER, AND R. V. PYLE, in *Plasma Physics and Controlled Nuclear Fusion Research 1971* (International Atomic Energy Agency, Vienna, 1971), Vol. II, p. 707.
11. F. H. COENSGEN, W. F. CUMMINS, V. A. FINLAYSON, W. F. NEXSEN, JR. AND T. C. SIMONEN, in *Plasma Physics and Controlled Nuclear Fusion Research 1971* (International Atomic Energy Agency, Vienna, 1971), Vol. II, p. 721.
12. R. D. RICHTMYER AND K. W. MORTON, "Difference Methods for Initial Value Problems," Wiley Interscience, New York, 1967.
13. J. DOUGLAS AND J. GUNN, *Numer. Math.* **6** (1964), 428, referred to hereafter as DG).